Precision Measurement of the Nickel Spectrum in Cosmic Rays from 8.8 GeV/n to 240 GeV/n with CALET on the International Space Station

O. Adriani,[1,2] Y. Akaike,[3,4,*] K. Asano,[5] Y. Asaoka,[5] E. Berti,[1,2] G. Bigongiari,[6,7,†] W.R. Binns,[8] M. Bongi,[1,2] P. Brogi,[6,7] A. Bruno,[9] J.H. Buckley,[8] N. Cannady,[10,11,12] G. Castellini,[13] C. Checchia,[6,‡] M.L. Cherry,[14] G. Collazuol,[15,16] K. Ebisawa,[17] A. W. Ficklin,[14] H. Fuke,[17] S. Gonzi,[1,2] T.G. Guzik,[14] T. Hams,[10] K. Hibino,[18] M. Ichimura,[19] K. Ioka,[20] W. Ishizaki,[5] M.H. Israel,[8] K. Kasahara,[21] J. Kataoka,[22] R. Kataoka,[23] Y. Katayose,[24] C. Kato,[25] N. Kawanaka,[26,27] Y. Kawakubo,[14] K. Kobayashi,[3,4] K. Kohri,[28] H.S. Krawczynski,[8] J.F. Krizmanic,[10,11,12] P. Maestro,[6,7] P.S. Marrocchesi,[6,7] A.M. Messineo,[29,7] J.W. Mitchell,[30] S. Miyake,[31] A.A. Moiseev,[32,11,12] M. Mori,[33] N. Mori,[2] H.M. Motz,[34] K. Munakata,[25] S. Nakahira,[17] J. Nishimura,[17] G.A. de Nolfo,[35] S. Okuno,[18] J.F. Ormes,[36] N. Ospina,[15,16] S. Ozawa,[37] L. Pacini,[1,13,2] P. Papini,[2] B.F. Rauch,[8] S.B. Ricciarini,[13,2] K. Sakai,[10,11,12] T. Sakamoto,[38] M. Sasaki,[32,11,12] Y. Shimizu,[18] A. Shiomi,[39] P. Spillantini,[1] F. Stolzi,[6,7,§] S. Sugita,[38] A. Sulaj,[6,7] M. Takita,[5] T. Tamura,[18] T. Terasawa,[40] S. Torii,[3] Y. Tsunesada,[41] Y. Uchihori,[42] E. Vannuccini,[2] J.P. Wefel,[14] K. Yamaoka,[43] S. Yanagita,[44] A. Yoshida,[38] K. Yoshida,[21] and W. V. Zober[8]

(CALET Collaboration)

[1] *Department of Physics, University of Florence, Via Sansone, 1 - 50019 Sesto, Fiorentino, Italy*
[2] *INFN Sezione di Florence, Via Sansone, 1 - 50019 Sesto, Fiorentino, Italy*
[3] *Waseda Research Institute for Science and Engineering, Waseda University, 17 Kikuicho, Shinjuku, Tokyo 162-0044, Japan*
[4] *JEM Utilization Center, Human Spaceflight Technology Directorate, Japan Aerospace Exploration Agency, 2-1-1 Sengen, Tsukuba, Ibaraki 305-8505, Japan*
[5] *Institute for Cosmic Ray Research, The University of Tokyo, 5-1-5 Kashiwa-no-Ha, Kashiwa, Chiba 277-8582, Japan*
[6] *Department of Physical Sciences, Earth and Environment, University of Siena, via Roma 56, 53100 Siena, Italy*
[7] *INFN Sezione di Pisa, Polo Fibonacci, Largo B. Pontecorvo, 3 - 56127 Pisa, Italy*
[8] *Department of Physics and McDonnell Center for the Space Sciences, Washington University, One Brookings Drive, St. Louis, MO 63130-4899, USA*
[9] *Heliospheric Physics Laboratory, NASA/GSFC, Greenbelt, Maryland 20771, USA*
[10] *Center for Space Sciences and Technology, University of Maryland, Baltimore County, 1000 Hilltop Circle, Baltimore, Maryland 21250, USA*
[11] *Astroparticle Physics Laboratory, NASA/GSFC, Greenbelt, Maryland 20771, USA*
[12] *Center for Research and Exploration in Space Sciences and Technology, NASA/GSFC, Greenbelt, Maryland 20771, USA*
[13] *Institute of Applied Physics (IFAC), National Research Council (CNR), Via Madonna del Piano, 10, 50019 Sesto, Fiorentino, Italy*
[14] *Department of Physics and Astronomy, Louisiana State University, 202 Nicholson Hall, Baton Rouge, LA 70803, USA*
[15] *Department of Physics and Astronomy, University of Padova, Via Marzolo, 8, 35131 Padova, Italy*
[16] *INFN Sezione di Padova, Via Marzolo, 8, 35131 Padova, Italy*
[17] *Institute of Space and Astronautical Science, Japan Aerospace Exploration Agency, 3-1-1 Yoshinodai, Chuo, Sagamihara, Kanagawa 252-5210, Japan*
[18] *Kanagawa University, 3-27-1 Rokkakubashi, Kanagawa, Yokohama, Kanagawa 221-8686, Japan*
[19] *Faculty of Science and Technology, Graduate School of Science and Technology, Hirosaki University, 3, Bunkyo, Hirosaki, Aomori 036-8561, Japan*
[20] *Yukawa Institute for Theoretical Physics, Kyoto University, Kitashirakawa Oiwakecho, Sakyo, Kyoto 606-8502, Japan*
[21] *Department of Electronic Information Systems, Shibaura Institute of Technology, 307 Fukasaku, Minuma, Saitama 337-8570, Japan*
[22] *Waseda Research Institute for Science and Engineering, Waseda University, 3-4-1 Okubo, Shinjuku, Tokyo 169-8555, Japan*
[23] *National Institute of Polar Research, 10-3, Midori-cho, Tachikawa, Tokyo 190-8518, Japan*
[24] *Faculty of Engineering, Division of Intelligent Systems Engineering, Yokohama National University, 79-5 Tokiwadai, Hodogaya, Yokohama 240-8501, Japan*
[25] *Faculty of Science, Shinshu University, 3-1-1 Asahi, Matsumoto, Nagano 390-8621, Japan*
[26] *Hakubi Center, Kyoto University, Yoshida Honmachi, Sakyo-ku, Kyoto, 606-8501, Japan*
[27] *Department of Astronomy, Graduate School of Science, Kyoto University, Kitashirakawa Oiwake-cho, Sakyo-ku, Kyoto, 606-8502, Japan*
[28] *Institute of Particle and Nuclear Studies, High Energy Accelerator Research Organization, 1-1 Oho, Tsukuba, Ibaraki, 305-0801, Japan*

[29] University of Pisa, Polo Fibonacci, Largo B. Pontecorvo, 3 - 56127 Pisa, Italy
[30] Astroparticle Physics Laboratory, NASA/GSFC, Greenbelt, MD 20771, USA
[31] Department of Electrical and Electronic Systems Engineering,
National Institute of Technology, Ibaraki College,
866 Nakane, Hitachinaka, Ibaraki 312-8508 Japan
[32] Department of Astronomy, University of Maryland, College Park, Maryland 20742, USA
[33] Department of Physical Sciences, College of Science and Engineering, Ritsumeikan University, Shiga 525-8577, Japan
[34] Faculty of Science and Engineering, Global Center for Science and Engineering,
Waseda University, 3-4-1 Okubo, Shinjuku, Tokyo 169-8555, Japan
[35] Heliospheric Physics Laboratory, NASA/GSFC, Greenbelt, MD 20771, USA
[36] Department of Physics and Astronomy, University of Denver, Physics Building,
Room 211, 2112 East Wesley Ave., Denver, CO 80208-6900, USA
[37] Quantum ICT Advanced Development Center, National Institute of Information and Communications Technology,
4-2-1 Nukui-Kitamachi, Koganei, Tokyo 184-8795, Japan
[38] College of Science and Engineering, Department of Physics and Mathematics,
Aoyama Gakuin University, 5-10-1 Fuchinobe, Chuo, Sagamihara, Kanagawa 252-5258, Japan
[39] College of Industrial Technology, Nihon University, 1-2-1 Izumi, Narashino, Chiba 275-8575, Japan
[40] RIKEN, 2-1 Hirosawa, Wako, Saitama 351-0198, Japan
[41] Division of Mathematics and Physics, Graduate School of Science,
Osaka City University, 3-3-138 Sugimoto, Sumiyoshi, Osaka 558-8585, Japan
[42] National Institutes for Quantum and Radiation Science and Technology, 4-9-1 Anagawa, Inage, Chiba 263-8555, JAPAN
[43] Nagoya University, Furo, Chikusa, Nagoya 464-8601, Japan
[44] College of Science, Ibaraki University, 2-1-1 Bunkyo, Mito, Ibaraki 310-8512, Japan

(Dated: December 22, 2021)

The relative abundance of nickel with respect to iron is by far larger than all other trans-iron elements, therefore it provides a favourable opportunity for a low background measurement of its spectrum. Since nickel, as well as iron, is one of the most stable nuclei, the nickel energy spectrum and its relative abundance with respect to iron provide important information to estimate the abundances at the source and to model the propagation of heavy nuclei. However, only a few direct measurements of cosmic-ray nickel at energy larger than $\sim$ 3 GeV/n are available at present in the literature and they are affected by strong limitations in both energy reach and statistics. In this paper we present a measurement of the differential energy spectrum of nickel from 8.8 GeV/n to 240 GeV/n, carried out with unprecedented precision by the Calorimetric Electron1 Telescope (CALET) in operation on the International Space Station since 2015. The CALET instrument can identify individual nuclear species via a measurement of their electric charge with a dynamic range extending far beyond iron (up to atomic number Z = 40). The particle's energy is measured by a homogeneous calorimeter (1.2 proton interaction lengths, 27 radiation lengths) preceded by a thin imaging section (3 radiation lengths) providing tracking and energy sampling. This paper follows our previous measurement of the iron spectrum [1] and it extends our investigation on the energy dependence of the spectral index of heavy elements. It reports the analysis of nickel data collected from November 2015 to May 2021 and a detailed assessment of the systematic uncertainties. In the region from 20 GeV/n to 240 GeV/n our present data are compatible within the errors with a single power law with spectral index -2.51 ± 0.07.

PACS numbers: 98.70.Sa, 96.50.sb, 95.55.Vj, 29.40.Vj, 07.05.Kf

INTRODUCTION

The energy spectra and relative abundances of cosmic rays (CR) are key observables for a theoretical understanding of the acceleration and propagation mechanisms of charged particles in our galaxy [2–16]. Direct measurements by space-borne instruments have recently achieved a level of unprecedented precision, thanks to long term observations and their capability to identify individual chemical elements. Direct measurements from high-altitude balloons and indirect measurements from ground based arrays convey important complementary information, albeit with different systematic uncertainties. The extension to higher energies of CR spectral data have shown unexpected deviations from a single power-law, as in the case of the recently observed double broken spectral shape of the proton spectrum in the multi-TeV domain, reported by DAMPE [17] and CALET [18]. A progressive spectral hardening has been established for light elements and heavier nuclei [19–23] with an onset at a few hundred GeV/n. The spectral study of heavy elements was recently extended to higher energies with the publication of the iron spectrum by AMS-02 [24] and CALET [1].

In this Letter, we pursue the study of elements sitting on the high side of the Periodic Table, where nickel – with much larger abundance than all other trans-iron elements – provides a favourable opportunity for a low

background measurement of its spectrum.

Space-borne direct measurements of CR nickel include the spectrum measured from 0.6 to 35 GeV/n by the French-Danish C2 instrument HEAO3-C2 [25] onboard the NASA HEAO3 satellite (launched in 1979) and the recent measurement by NUCLEON (launched in 2014) [26] in the energy range $\sim 51 - 511$ GeV/n. Measurements in the lower energy range 50 – 550 MeV/n were carried out, during the 2009 – 2010 solar minimum period, by the Cosmic Ray Isotope Spectrometer (CRIS) [27] onboard the Advanced Composition Explorer at the L1 Lagrangian point. Data up to ~ 500 MeV/n [28] were collected by *Voyager 1* after the start of observations of the local interstellar energy spectra of Galactic cosmic-ray nuclei (August 2012).

Earlier measurements with balloon experiments have a limited statistics and energy reach. They include: (i) the High Energy Nuclei telescope (HEN) [29] at nickel energies up to about 10.5 GeV/n (3 flights in 1971 and 1972 for a total of 7.6 m^2 sr hours); (ii) the scintillation-Cherenkov telescope (hereafter cited as Balloon 1975) [30] from 1 to 10 GeV per amu (2 flights in 1975 with a total exposure of 20 m^2 sr hr); (iii) the multi-element Cherenkov telescope [31] from 0.3 – 50 GeV/n (3 flights in 1974 and one in 1976); (iv) the Cosmic Ray Isotope Instrument System (CRISIS) [32] from 600 – 900 MeV/n ($\sim$ 57 hrs afloat in 1975); (v) the Large Isotopic Composition Experiment (ALICE) [33] at energies near 1 GeV/n (flown for 14.7 hours in 1987).

In this Letter we present a measurement of the differential energy spectrum of CR nickel from 8.8 GeV/n to 240 GeV/n carried out, with unprecedented precision, with CALET onboard the International Space Station (ISS). Though optimized for the measurement of the all-electron spectrum [34, 35], CALET has an excellent charge identification capability to tag individual CR elements [36–39] from proton to nickel (and above). It can explore particle energies up to the PeV scale thanks to its large dynamic range, adequate calorimetric depth and accurate tracking. CALET published accurate spectral measurements of electrons [35], protons [36], carbon [23], oxygen [23], and iron [1]. Preliminary updates of proton, helium, boron and B/C analyses were presented at the ICRC-2021 conference [40].

CALET INSTRUMENT

Charge identification is carried out by the CHarge Detector (CHD), a two-layered hodoscope of plastic scintillator paddles. It can resolve individual elements from atomic number Z = 1 to Z = 40 with excellent charge resolution [41]. The particle's energy is measured with the TASC (Total AbSorption Calorimeter), a lead-tungstate homogeneous calorimeter (27 radiation lengths (r.l.), 1.2 proton interaction lengths) preceded by a thin (3 r.l.) pre-shower IMaging Calorimeter (IMC). The latter is equipped with 16 layers of thin scintillating fibers (1 mm^2 square cross-section) and interleaved with tungsten absorbers read out individually. The IMC provides tracking capabilities as well as an independent charge measurement, via multiple samples of specific energy loss (dE/dx) in each fiber, up to the onset of saturation which occurs for ions above silicon. Therefore charge identification for nickel and neighboring elements relies on CHD only. More details on the instrument and on the trigger system can be found in the Supplemental Material (SM) of Ref. [34]. CALET was launched on August 19, 2015 and installed on the Japanese Experiment Module Exposure Facility of the ISS. The on-orbit commissioning phase was successfully completed in the first days of October 2015. Calibration and test of the instrument took place at the CERN-SPS during five campaigns between 2010 and 2015 with beams of electrons, protons and relativistic ions [42–44].

DATA ANALYSIS

The flight data (FD) used in the present analysis were collected over a period of 2038 days of CALET operation. The total observation live time for the high-energy (HE) shower trigger [45] is $T \sim 4.1 \times 10^4$ hours, corresponding to 86.0% of total observation time.

Individual on-orbit calibration of all channels are performed with a dedicated trigger mode [44, 45] allowing the selection of penetrating protons and He particles. First, raw data are corrected for gain differences among the channels, light output non-uniformity and any residual dependence on time and temperature. After calibration, a single "best track" is reconstructed for each event with an associated estimate of its charge and energy.

The particle's direction and entrance point are reconstructed from the coordinates of the scintillating fibers in the IMC. The tracking algorithm, based on a combinatorial Kalman filter, identifies the incident track in the presence of background hits generated by backscattered radiation from the TASC [46]. The angular resolution and the spatial resolution for the impact point on the CHD are $\sim 0.08^\circ$ and $\sim$180 μm respectively.

Physics processes and interactions in the apparatus are simulated via Monte Carlo (MC) techniques, based on the EPICS package [47, 48] which implements the hadronic interaction model DPMJET-III [49]. The instrument configuration and detector response are detailed in the simulation code which provides digitized signals from all channels. An independent analysis based on GEANT4 [50] is also performed to assess the systematic uncertainties. In this analysis, only ^{58}Ni isotope was considered since its mass difference with respect to other isotopes (mainly ^{60}Ni) is less than 3%.

Charge measurement The particle's charge Z is

reconstructed from the signals of the CHD paddles traversed by the incident particle and properly corrected for its path length. Either CHD layer provides an independent dE/dx measurement which has to be corrected for the quenching effect in the scintillator's light yield. The latter is parameterized by fitting selected FD samples of each nuclear species to a "halo" model [41] as a function of Z^2. The resulting curves are then used to reconstruct a charge value in either layer ($Z_{\rm CHDX}$, $Z_{\rm CHDY}$) on an event-by-event basis [23]. The presence of an increasing amount of backscatters from the TASC at higher energy generates additional energy deposits in the CHD that add on to the primary particle ionization signal and may induce a wrong charge identification. This effect causes a systematic displacement of the CHDX/CHDY charge peaks to higher values (up to 0.8 charge units) with respect to the nominal charge position. Therefore it is necessary to restore the nickel peak position to its nominal value, Z = 28, by an energy dependent charge correction applied separately to the FD and the MC data. A similar correction is applied to iron and nearby elements. The CHD charge resolution σ_Z, obtained combining the average of $Z_{\rm CHDX}$ and $Z_{\rm CHDY}$ signal is 0.39 in charge units and it is shown in Fig. S1 of the SM [51]. Background contamination from neighbor elements misidentified as nickel is shown in Fig. S2 of the SM [51]. Between 100 GeV and 1 TeV it is mainly due to iron and secondly to cobalt. Above 1 TeV the iron contribution is dominant. Contamination from heavier nuclei is negligible.

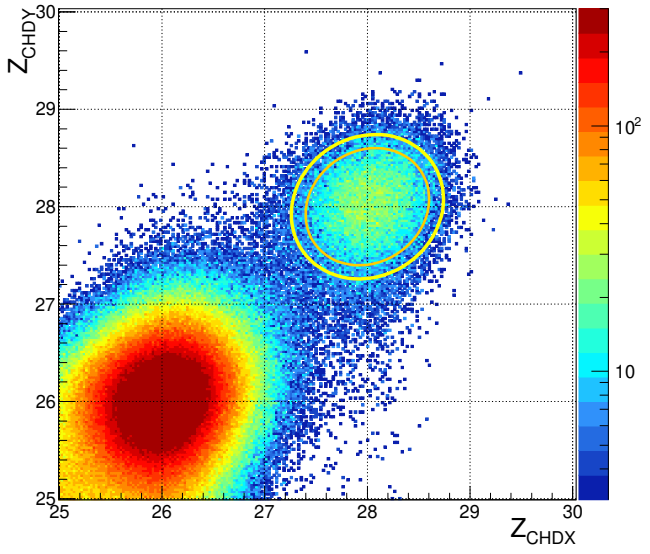

FIG. 1. Crossplot of $Z_{\rm CHDY}$ vs. $Z_{\rm CHDX}$ reconstructed charges in the elemental range between Mn (Z = 25) and Zn (Z = 30). Nickel candidates are selected inside an ellipse with minor and major semi-axes 1.4 σ_x and 1.4 σ_y, respectively, rotated clockwise by 45°. The maximum and the minimum elliptical selection (depending on the energy) are indicated by the yellow and the orange ellipses in the figure.

Energy measurement For each event, the shower energy $E_{\rm TASC}$ is calculated as the sum of the energy deposits of all TASC logs, after merging the calibrated gain ranges of each channel [45]. The energy response derived from the MC simulations was tuned using the results of a beam test carried out at the CERN-SPS in 2015 [42] with beams of accelerated ion fragments of 13, 19 and 150 GeV/c/n momentum per nucleon (as described in the SM of Ref. [23]). Correction factors are 6.7% for $E_{\rm TASC} < 45$ GeV and 3.5% for $E_{\rm TASC} > 350$ GeV, respectively. A linear interpolation is used to determine the correction factor for intermediate energies.

Event selection The onboard HE shower trigger, based on the coincidence of the summed dynode signals of the last four IMC layers and the top TASC layer (TASCX1) is fully efficient for elements heavier than oxygen. Therefore, an offline trigger confirmation, as required for the analysis of lower charge elements [23, 36], is not necessary for nickel, because the HE trigger threshold is far below the signal amplitude expected from a nickel ion at minimum ionization (MIP) and the trigger efficiency is close to 100%. However, in order to select interacting particles, a deposit larger than 2 sigmas of the MIP peak is required in at least one of the first four layers of the TASC.

Events with one well-fitted track crossing the whole detector from the top of the CHD to the TASC bottom layer (and clear from the edges of TASCX1 by at least 2 cm) are selected. The fiducial geometrical factor for this category of events is $S\Omega \sim 510\,{\rm cm}^2{\rm sr}$, corresponding to about 50% of CALET total acceptance.

Particles undergoing a charge-changing nuclear interaction in the upper part of the instrument are removed by requiring that the difference between the charges from either layer of the CHD is less than 1.5 charge units. The cross plot of the $Z_{\rm CHDY}$ vs. $Z_{\rm CHDX}$ charge, in Fig. 1, shows the nickel events selection: candidates are contained within an ellipse centred at Z = 28 with 1.4 σ_x and 1.4 σ_y wide semiaxes (with both variances depending on the energy) for $Z_{\rm CHDX}$ and $Z_{\rm CHDY}$, respectively, and rotated clockwise by 45°. Event selections are identical for the MC and the FD.

Energy unfolding As detailed in Ref. [1] for iron, the TASC crystals are subject to a light quenching phenomenon which is not reproduced by the MC simulations. Therefore a quenching correction is extracted from the FD and applied *a posteriori* to the MC energy deposits generated by non-interacting primary particles in the TASC logs. Distributions of $E_{\rm TASC}$ for Ni selected candidates are shown in Fig. S2 of the SM [51], with a sample of 5.2×10^3 events.

In order to take into account the limited calorimetric energy resolution for hadrons (of the order of ∼30%) an energy unfolding algorithm is applied to correct for bin-to-bin migration effects. In this analysis, we used the Bayesian approach [52] implemented within the RooUnfold package [53] of the ROOT analysis framework [54]. Each element of the response matrix represents the prob-

ability that a primary nucleus in a given energy interval of the CR spectrum produces an energy deposit falling into a given bin of $E_{\rm TASC}$. The response matrix is derived using the MC simulation after applying the same selection procedure as for flight data and it is shown in Fig. S6 of the SM [51].

Differential energy spectrum The energy spectrum is obtained from the unfolded energy distribution as follows:

$$\Phi(E) = \frac{N(E)}{\Delta E\ \varepsilon(E)\ S\Omega\ T} \tag{1}$$

$$N(E) = U\left[N_{obs}(E_{\rm TASC}) - N_{bg}(E_{\rm TASC})\right] \tag{2}$$

where ΔE denotes the energy bin width, E is the geometric mean of the lower and upper bounds of the bin [55], $N(E)$ the bin content in the unfolded distribution, $\varepsilon(E)$ the total selection efficiency (Fig. S3 of the SM [51]), $U()$ the unfolding procedure operator, $N_{obs}(E_{\rm TASC})$ the bin content of observed energy distribution (including background), and $N_{bg}(E_{\rm TASC})$ the bin content of background events in the observed energy distribution. In the energy range between 10^2 GeV and 10^3 GeV of $E_{\rm TASC}$ the background fraction is $N_{bg}/N_{obs} \sim 1\%$. Starting from 10^3 GeV it increases up to 10% at 10^4 GeV.

SYSTEMATIC UNCERTAINTIES

Dominant sources of systematics uncertainties in the nickel analysis are due to MC model and event selection at high energy. The systematic error related to charge identification was studied by varying the semi-axes of the elliptical selection up to ±15%. The result was an (energy bin dependent) flux variation lower than 4% below 100 GeV/n and increasing to $\sim$ 8% at 200 GeV/n. A comparison between different MC is in order as it is not possible to validate the MC simulations with beam test data at high energy. A comparative study of key distributions was carried out with EPICS and GEANT4 showing that the respective total selection efficiencies for Ni are in agreement within $\sim$ 3% over the whole energy range (Fig. S3 of the SM [51]). The difference between the two energy response matrices is comprised between -5% and +5%. The resulting fluxes show a difference around $\sim$ 5% below 40 GeV/n and less than $\sim$ 10% in the 100 – 200 GeV/n region.

The uncertainty on the energy scale correction is ±2% and depends on the accuracy of the beam test calibration. It causes a rigid shift of the flux (±4%) above 30 GeV/n, not affecting the spectral shape. As the beam test model was not identical to the instrument in flight [36], the difference in the spectrum (±5% up to 140 GeV/n) obtained with either configuration was modeled and included in the systematic error.

The uncertainties due to the unfolding procedure were evaluated with different response matrices computed by varying the spectral index (between -2.9 and -2.2) of the MC generation spectrum.

As the trigger threshold is much smaller than the energy of a non interacting nickel, the HE trigger efficiency is close to 100% in the whole energy range with a negligible contribution to the systematic error. The fraction of interactions (Fig. S5 of the SM [51]) in the CHD, and above it, was checked by comparing the MC and the FD as explained in the SM. The contribution due to a shower event cut, rejecting non interacting particles (4% around 10 GeV and 2% above), was evaluated and included in the systematic uncertainties.

Possible inaccuracy of track reconstruction could affect the determination of the geometrical acceptance. The contamination due to off-acceptance events that are erroneously reconstructed inside the fiducial acceptance was estimated by MC to be $\sim$ 1% at 10 GeV/n while decreasing to less than 0.1% above 60 GeV/n. The systematic uncertainty on the tracking efficiency is negligible [23]. A different tracking procedure, described in Ref. [56], was also used to study possible systematic uncertainties in tracking efficiency. The result is well consistent with the Kalman filter algorithm. The systematic error related to background contamination is assessed by varying the contamination level by as much as ±50%. The result was a flux variation around 1% below 100 GeV/n, increasing to 3% at 200 GeV/n.

Additional energy-independent systematic uncertainties affecting the flux normalization include live time (3.4%), long-term stability ($< 2.7\%$) and geometrical factor ($\sim 1.6\%$), as detailed in the SM of Ref. [34]. The energy dependence of all systematic errors for nickel analysis is shown in Fig. S8 of the SM [51]. The total systematic error is computed as the sum in quadrature of all the sources of systematics in each energy bin.

RESULTS

The nickel differential spectrum in kinetic energy per nucleon measured by CALET from 8.8 GeV/n to 240 GeV/n is shown in Fig. 2, where current uncertainties including statistical and systematic errors are bounded within a green band. The CALET spectrum is compared with the results from Balloon 1975 [30], CRISIS [32], HEAO3-C2 [25] and NUCLEON [26]. The nickel flux measurements with CALET are tabulated in Table I of the SM [51] where statistical and systematic errors are also shown. CALET and HEAO3-C2 nickel spectra have similar flux normalization in the common interval of energies. CALET and NUCLEON differ in the shape although the two measurements show a similar flux normalization at low energy.

Figure 3 shows a fit to the CALET nickel flux with a

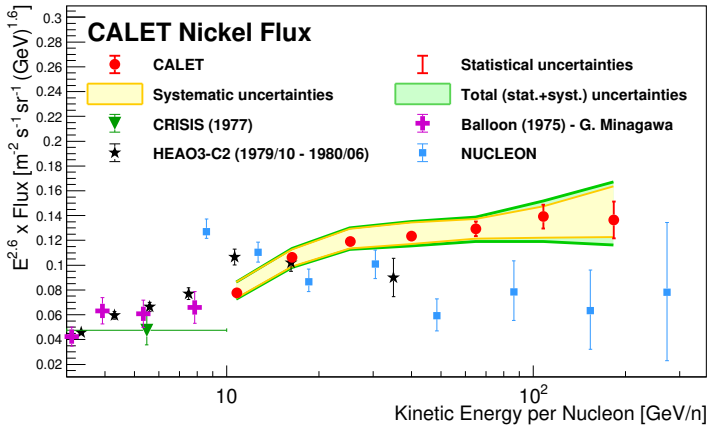

FIG. 2. CALET nickel flux (multiplied by $E^{2.6}$) as a function of kinetic energy per nucleon. Error bars of the CALET data (red) represent the statistical uncertainty only, the yellow band indicates the quadrature sum of systematic errors, while the green band indicates the quadrature sum of statistical and systematic errors. Also plotted are the measurements from Balloon 1975 [30], CRISIS [32], HEAO3-C2 [25] and NUCLEON [26]. This figure is reproduced enlarged in Fig. S9 of the SM [51].

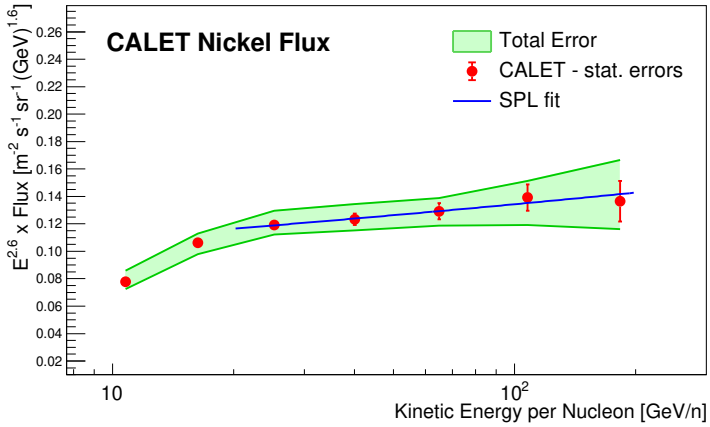

FIG. 3. Fit of the CALET nickel energy spectrum to an SPL function (blue line) in the energy range [20, 240] GeV/n. The flux is multiplied by $E^{2.6}$ where E is the kinetic energy per nucleon. The error bars are representative of purely statistical errors.

single power law function (SPL)

$$\Phi(E) = C \left(\frac{E}{1\ \mathrm{GeV}} \right)^{\gamma} \qquad (3)$$

where γ is the spectral index and C is the normalization factor.

The fit is performed from 20 GeV/n to 240 GeV/n and gives $\gamma = -2.51 \pm 0.04(\mathrm{stat}) \pm 0.06(\mathrm{sys})$ with $\chi^2/\mathrm{d.o.f.} = 0.3/3$. To better understand the nickel spectral behavior we report also the nickel to iron ratio as a function of kinetic energy per nucleon (see Fig. 4). Our measure extends the results of previous experiments (i.e. HEAO3-C2) up to 240 GeV/n. The fit, performed from 8.8 GeV/n to 240 GeV/n, gives a constant value of $0.061 \pm 0.001(\mathrm{stat})$ with the $\chi^2/\mathrm{d.o.f.} = 2.3/6$.

The experimental limitations of the present measurement (i.e. low statistics as well as large systematic errors for the highest energy bins) do not allow yet to test the hypothesis of a spectral shape different from a single power law. As a matter of fact, current expectations (e.g., [6, 9]) for a detectable spectral hardening of nickel are still under debate.

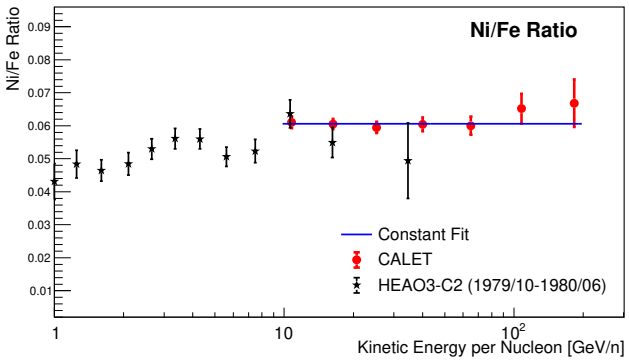

FIG. 4. Nickel to iron flux ratio measured with CALET (red points). The errors bars are representative of statistical errors only. Data are fitted with a constant function giving Ni/Fe = 0.061 ± 0.001. Also plotted is the result from HEAO3-C2 [25].

CONCLUSION

In this paper, based on 67 months of observations with CALET on the ISS, we report for the first time a measurement of the energy spectrum of nickel over an extended energy range up to 240 GeV/n and with a significantly better precision than most of the existing measurements. Above 20 GeV/n, our present observations are consistent with the hypothesis of an SPL spectrum up to 240 GeV/n. Beyond this limit, the uncertainties given by our present statistics and large systematics do not allow us to draw a significant conclusion on a possible deviation from a single power law. An SPL fit in this region yields a spectral index value $\gamma = -2.51 \pm 0.07$. The flat behavior of the nickel to iron ratio suggests that the spectral shape of Fe and Ni is the same within the experimental accuracy. This suggests a similar acceleration and propagation behaviour as expected from small difference in atomic number and weight between Fe and Ni nuclei. An extended data set, as expected beyond the 67 months period of continuous observations accomplished so far, will not only improve the dominant statistical limitations of the present measurement, but also our understanding of the instrument response in view of a further reduction of systematic uncertainties.

ACKNOWLEDGMENTS

We gratefully acknowledge JAXA's contributions to the development of CALET and to the operations

aboard the JEM-EF on the International Space Station. We also wish to express our sincere gratitude to ASI (Agenzia Spaziale Italiana) and NASA for their support of the CALET project. This work was supported in part by KAKENHI Grant Numbers 26220708, 19H05608, 17H02901, 21K03592, and 20K22352 and by the MEXT-Supported Program for the Strategic Research Foundation at Private Universities (2011-2015) (No.S1101021) at Waseda University. The CALET effort in Italy is supported by ASI under agreement 2013-018-R.0 and its amendments. The CALET effort in the United States is supported by NASA through Grants No. 80NSSC20K0397, No. 80NSSC20K0399, and No. NNH18ZDA001N-APRA18-0004.

* yakaike@aoni.waseda.jp
† bigongiari2@unisi.it
‡ caterina.checchia2@unisi.it
§ francesco.stolzi@unisi.it

[1] O. Adriani *et al.* (CALET), Phys. Rev. Lett. **126**, 241101 (2021).
[2] L. O. Drury, Mon. Not. R. Astron. Soc. **415**, 1807 (2011).
[3] Y. Ohira and K. Ioka, Astrophys. J. Lett. **729**, L13 (2011).
[4] M. A. Malkov, P. H. Diamond, and R. Z. Sagdeev, Phys. Rev. Lett. **108**, 081104 (2012).
[5] P. Blasi, E. Amato, and P. D. Serpico, Phys. Rev. Lett. **109**, 061101 (2012).
[6] N. Tomassetti, Astrophys. J. Lett. **752**, L13 (2012).
[7] A. Vladimirov, G. Johannesson, I. Moskalenko, and T. Porter, Astrophys. J. **752**, 68 (2012).
[8] V. Ptuskin, V. Zirakashvili, and E. S. Seo, Astrophys. J. **763**, 47 (2013).
[9] S. Thoudam and J. R. Hörandel, Astron. Astrophys. **567**, A33 (2014).
[10] G. Bernard *et al.*, Astron. Astrophys. **555**, A48 (2013).
[11] P. Serpico, in *Proceedings of Science (ICRC2015) 009* (2015).
[12] Y. Ohira, N. Kawanaka, and K. Ioka, Phys. Rev. D **93**, 083001 (2016).
[13] C. Evoli, P. Blasi, G. Morlino, and R. Aloisio, Phys. Rev. Lett. **121**, 021102 (2018).
[14] C. Evoli, R. Aloisio, and P. Blasi, Phys. Rev. D **99**, 103023 (2019).
[15] K. Caprioli *et al.*, in *Proceedings of Science (ICRC2021) 482* (2021).
[16] P. Lipari, in *Proceedings of Science (ICRC2021) 169* (2021).
[17] Q. An *et al.* (DAMPE), Sci. Adv. **5**, eaax3793 (2019).
[18] K. Kobayashi and P. S. Marrocchesi, in *Proceedings of Science (ICRC2021) 098* (2021).
[19] M. Aguilar *et al.* (AMS), Phys. Rev. Lett. **119**, 251101 (2017).
[20] M. Aguilar *et al.* (AMS), Phys. Rev. Lett. **120**, 021101 (2018).
[21] M. Aguilar *et al.* (AMS), Phys. Rev. Lett. **124**, 211102 (2020).
[22] H. S. Ahn *et al.* (CREAM), Astrophys. J. Lett. **714**, L89 (2010).
[23] O. Adriani *et al.* (CALET), Phys. Rev. Lett. **125**, 251102 (2020).
[24] M. Aguilar *et al.* (AMS), Phys. Rev. Lett. **126**, 041104 (2021).
[25] J. J. Engelmann *et al.* (HEAO3-C2), Astron. Astrophys. **233**, 96 (1990).
[26] V. Grebenyuk *et al.* (NUCLEON), (2018), arXiv:1809.07285 [astro-ph.HE].
[27] K. A. Lave *et al.*, **770**, 117 (2013).
[28] A. C. Cummings *et al.*, Astrophys. J. **831**, 18 (2016).
[29] E. Juliusson, Astrophys. J. **191**, 331 (1974).
[30] G. Minagawa, Astrophys. J. **248**, 847 (1981).
[31] J. A. Lezniak and W. R. Webber, Astrophys. J. **223**, 676 (1978).
[32] J. S. Young *et al.*, Astrophys. J. **246**, 1014 (1981).
[33] J. Esposito *et al.*, Astroparticle Physics **1**, 33 (1992).
[34] O. Adriani *et al.* (CALET), Phys. Rev. Lett. **119**, 181101 (2017).
[35] O. Adriani *et al.* (CALET), Phys. Rev. Lett. **120**, 261102 (2018).
[36] O. Adriani *et al.* (CALET), Phys. Rev. Lett. **122**, 181102 (2019).
[37] S. Torii and P. S. Marrocchesi (CALET), Adv. Space Res. **64**, 2531 (2019).
[38] S. Torii (CALET), in *Proceedings of Science (ICRC2017) 1092* (2017).
[39] Y. Asaoka (CALET), in *Proceedings of Science (ICRC2019) 001* (2019).
[40] P. S. Marrocchesi, PoS **ICRC2021**, 010 (2021).
[41] P. S. Marrocchesi *et al.*, Nucl. Instr. and Meth. A **659**, 477 (2011).
[42] Y. Akaike (CALET), in *Proceedings of Science (ICRC2015) 613* (2015).
[43] G. Bigongiari (CALET), in *Proceedings of Science (ICRC2015) 592* (2015).
[44] T. Niita *et al.* (CALET), Adv. Space Res. **55**, 2500 (2015).
[45] Y. Asaoka *et al.* (CALET), Astroparticle Physics **91**, 1 (2017).
[46] P. Maestro and N. Mori (CALET), in *Proceedings of Science (ICRC2017) 208* (2017).
[47] K. Kasahara, in *Proc. of 24th international cosmic ray conference (Rome, Italy)*, Vol. 1 (1995) p. 399.
[48] See EPICS webpage `http://cosmos.n.kanagawa-u.ac.jp/EPICSHome/`.
[49] S. Roesler, R. Engel, and J. Ranft, in *Proceedings of the Monte Carlo Conference, Lisbon, 1033-1038* (2000).
[50] J. Allison *et al.*, Nuclear Instruments and Methods in Physics Research Section A: Accelerators, Spectrometers, Detectors and Associated Equipment **835**, 186 (2016).
[51] See the Supplemental Material at `http://PRL/` for supporting figures and the tabulated fluxes, as well as the description of data analysis procedure and the detailed assessment of systematic uncertainties.
[52] G. D'Agostini, Nucl. Instr. and Meth. A **362**, 487 (1995).
[53] T. Adye, (2011), arXiv:1105.1160.
[54] R. Brun and R. Rademarkers, Nucl. Instr. and Meth. A **389**, 81 (1997).
[55] D. Maurin, H. P. Dembinski, J. Gonzalez, I. C. Mariș, and F. Melot, Universe **6**, 102 (2020).
[56] Y. Akaike (CALET), IOP Conf. Series: Journal of Physics: Conf. Series **1181**, 012042 (2019).